Journal of Hydrology: Regional Studies 32 (2020) 100750

Contents lists available at ScienceDirect

Journal of Hydrology: Regional Studies

journal homepage: www.elsevier.com/locate/ejrh

Exploring causes of streamflow alteration in the Medjerda river, Algeria

Mokrane Kadir [a,*], Raed Fehri [a], Doudja Souag [b], Marnik Vanclooster [a]

[a] Université catholique de Louvain, Earth and Life Institute (ELI), GERU, Croix du Sud 2, 1348 Louvain-la-Neuve, Belgium
[b] LEGHYD Laboratory, University of Science and Technology Houari Boumediene, BP 32, Bab Ezzouar, Algiers, Algeria

ARTICLE INFO

Keywords:
Causality
CCM
Hydrological alteration
Medjerda river
Trends

ABSTRACT

Study region: The Medjerda is a transboundary catchment located in North-Eastern Algeria and shared with Tunisia.
Study focus: In this study, we explore the causes of hydrological alteration of streamflow in a sub-catchment of the Medjerda in Algeria. The hydrological alteration was explored through the application of Mann-Kendall test based on possible explanatory factors, namely, precipitation, evapotranspiration, temperature, irrigation, and Normalized Difference of Vegetation Index (NDVI). Furthermore, the causal factors of streamflow variation were addressed using Convergent Cross Mapping (CCM) method.
New hydrological insights for the region: Results of the trend analysis yield that the streamflow is altered during the period 1981−2012. This is consistent with the trends of the possible explanatory factors of this alteration. The Convergent Cross Mapping (CCM) method showed that streamflow alteration is unidirectionally caused by changes in patterns of precipitation, temperature, evapotranspiration, irrigation, and NDVI, and that there is little feedback from streamflow alteration to these causing factors. Overall, our assessment showed that the method used to identify the causal relationships in dynamical systems based on the CCM algorithm is suitable for exploring the drivers of the hydrologic alteration in multivariate time series, in particular when nonlinear dynamics determine the system.

1. Introduction

The hydrological regime of a river strongly controls its different functions and ecosystem services. Land cover and climate change may significantly alter the hydrological regime (Milly et al., 2005; Barnett et al., 2005; Cohen Liechti et al., 2014), particularly in areas characterized by arid and semi-arid climates such as the Mediterranean region (Schilling et al., 2012). In this region, rainfall regimes have been altered by climatic and/or physiographic characteristics, strongly affecting the streamflow regime (Zamoum and Souag-Gamane, 2019). Within the Mediterreann region, Algeria and Tunisia are considered as highly water stressed countries, suffering from extreme water scarcity in recent decades (FAO, 2018; Schilling et al., 2012). Indeed, Algeria is facing low precipitation affected by high spatial and temporal variability, low runoff, high evapotranspiration, and increased drought severity, which will significantly reduce the streamflow of rivers. The potential effects of climate change are expected to increase current pressures on water resources (Sellami et al., 2016). As a result, surface water and groundwater will be reduced with a direct effect on the allocation

* Corresponding author.
E-mail address: mokrane.kadir@uclouvain.be (M. Kadir).

https://doi.org/10.1016/j.ejrh.2020.100750
Received 17 March 2020; Received in revised form 8 October 2020; Accepted 12 October 2020
Available online 2 November 2020

of water among sectors (irrigation, water supply, and industry) (FAO, 2018). However, climate change includes also alterations in temperature, evapotranspiration, vapor pressure, and wind speed regimes that could conduct to structural changes of streamflow indirectly. In addition, other factors like land cover change, dam construction, and irrigation development, also contribute to the hydrological alteration.

Understanding the role of each possible causal factor on the hydrological alteration is pivotal and plays an important role in the agricultural development of the whole region. The identification of the causal factors and their specific contribution to the hydrological alteration remains a challenging task.

Several studies used correlation tests in multivariate time series to study causality including hydro-climatic variables like temperature (T), precipitation (P), wind speed (WS), evapotranspiration (ET), relative humidity (H), soil moisture (SM), Normalized Difference of Vegetation Index (NDVI), and streamflow (Q) (Meng et al., 2014; Khazaei et al., 2019; Miao et al., 2011). However, the correlation criterion does not necessarily imply causation and vice versa. It is neither necessary nor powerful for establishing a causal map of factors in multivariate time series contributing to the hydrologic alteration, in particular when nonlinear dynamics determine the system (Van Nes et al., 2015; Duan et al., 2018). An alternative approach to identify causal relationships in dynamical systems is based on the Convergent Cross Mapping (CCM) algorithm. This approach is based on the theory of nonlinear dynamical systems developed by Takens (1981). The CCM has recently been introduced in hydroclimatology to detect the causal effects of soil moisture on precipitation (Duan et al., 2018), to quantify causal feedbacks in climate change (Van Nes et al., 2015), and to detect the causality of individual meteorological factors on local atmospheric pollution in China (Gao et al., 2017). The CCM algorithm is particularly suitable to extract causality links from mirage correlation (Sugihara et al., 2012). The CCM method has also the ability to detect time-delayed causality and to distinguish causality in both directions from the phenomenon of synchrony influenced by strong unidirectional causation (Ye et al., 2015). Yet, the efficiency and robustness of CCM algorithm compared to other causality detection methods need to be further explored.

The current study includes a comprehensive research on the detection of causal factors and their role on streamflow variations for an Algerian sub-catchment of the Medjerda catchment. The Medjerda basin is a Tunisian-Algerian transboundary basin subjected to hydrological alteration and water stress (Fehri et al., 2019). The economy of the Medjerda catchment depends largely on irrigated agriculture (Bouraoui et al., 2005). The assessment of the hydrological alteration, in addition to the identification of the causal factors using the CCM algorithm would be most valuable for long-term water resources planning and management within the region. The main objectives of this study are: (1) to investigate the hydrological alteration of the Medjerda river by assessing long term time series of

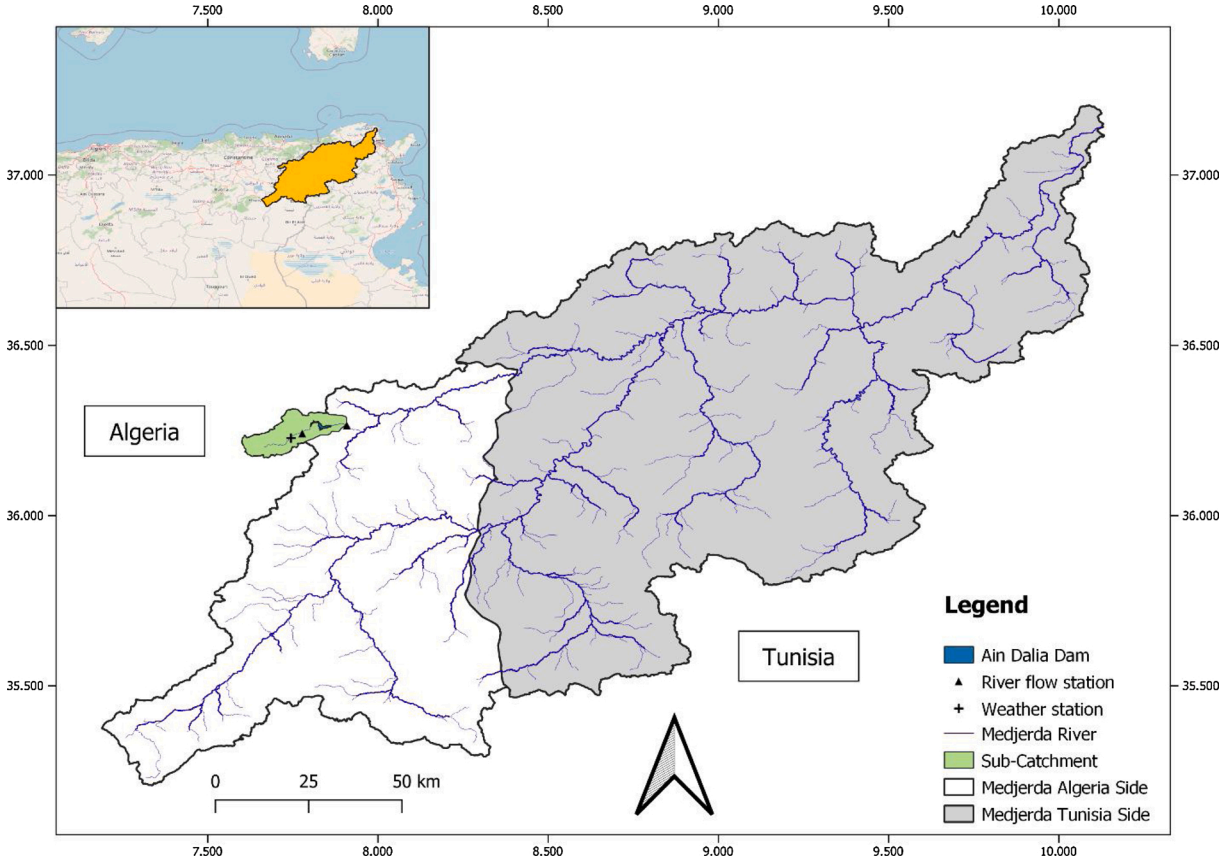

Fig. 1. Location of the study area.

possible explanatory factors using Mann-Kendall change detection and trend analysis technic; and (2) to identify and explain the causal relationships between possible explanatory factors and river flow using the CCM algorithm.

2. Study area

The Medjerda basin is located in northeast of Algeria and northwest of Tunisia. The Medjerda river is the longest river of the Tunisian-Algerian transboundary basin, with a total length of 485 km among which 135 km are situated in Algeria. The upstream part of the river basin is situated in the mountains of eastern Algeria and includes Ras Alia mountain with a height of 1317 m. The river subsequently flows into the northern part of Tunisia and discharges in the Mediterranean sea. The Medjerda basin has a total surface of 23 700 km^2 among which 7 870 km^2 are located in Algeria (Fig. 1). The water regime is typically Mediterranean with a large mean seasonal flow variability. The climate of the Medjerda is characterized by a continental climate with Mediterranean influence, with warm summers and cold winters. Agriculture is the main economic activity within the Medjerda basin. The Medjerda basin suffers from lack of consistent water management strategies, and is highly affected by climate change and of water stress. Fehri et al. (2019) showed that the level water stress reached 98 % in 2012. Upstream, in the Algerian side of the basin, the Ain Dalia dam was built in 1987 along the mainstream. The dam has a total capacity of 82 million m^3 and is principally used for drinking and irrigation water supply. In order to eliminate the anthropogenic effects of the dam construction in the analysis, we limit the analysis to the sub-catchment upstream of the Ain Dalia dam.

3. Materials and methods

3.1. Data sources

In this study, a long-term hydroclimatic and environmental database was constructed from different sources. The meteorological data were collected from a weather station monitored by the National Meteorological Office (NMO) of Algeria that included precipitation and mean air temperature. With respect to streamflow, data were collected from a gauging station monitored by the National Agency of Hydraulic Resources (ANRH) (Table 1) (Fig. 1). The hydroclimatic database was enriched with time series on ET and NDVI, both obtained from the Google Earth Engine (GEE) cloud-based platform (Table 1). The MODIS-ET data is provided by the Land Processes Distributed Active Archive Center (LP-DAAC) and estimates the terrestrial evapotranspiration at global scale. The ET estimates are computed following Mu et al. (2011), based on the Penman-Monteith equation (Monteith, 1965) at 500 m spatial resolution and at 8-day time step. In our case, data were aggregated at a monthly scale. This product can be used to determine regional water and energy balances and the soil water status of basins. Hence, it provides key information for water resource management.

The annual Land Cover (LC) maps were developed by the European Space Agency Climate Change Initiative (ESA-CCI) (Hollmann et al., 2013) available at (https://maps.elie.ucl.ac.be/CCI/viewer/). This dataset provides and describes continuous land cover changes at 300 m spatial resolution on a global scale from 1992 to 2015 (Li et al., 2018).

In order to evaluate irrigation water consumption (IRRI) at yearly scale, the MODIS-ET-500 m remote sensing product was combined with land cover data (irrigated lands) (Fig. 2).

Time series of NDVI were inferred from the Landsat 5 Top of Atmosphere (TOA) product. The NDVI is generated from the Near-IR and Red bands (i.e. NDVI = (NIR - Red) / (NIR + Red)) and ranges from -1.0 to 1.0. The NDVI data were created using Google Earth Engine (GEE), at 30 m spatial resolution and at monthly time scale for the entire Medjerda basin.

3.2. Assessing water consumption for irrigation water supply

In the study area, water is pumped intensively mainly from the Medjerda river and from aquifers for irrigation water supply. This water pumping may be another causing factor of hydrological alteration and need therefore to be assessed. However, the official information about irrigation water withdrawal is not available. Yang et al. (2018) showed that water consumption of different ecosystems could be estimated using different remote sensing evapotranspiration products. Furthermore, Zhao et al. (2018) and Fehri et al. (2019) used MODIS-ET product as a surrogate for irrigation water consumption. Therefore, in this study, this product was adopted to estimate water consumption for irrigation in the Medjerda sub-catchment. Irrigated lands were identified from the land cover map (CCI-LC 300 m).

Irrigated lands and ET (Fig. 2) were combined in order to estimate monthly and yearly irrigation water consumption for the period

Table 1
Information on hydroclimatic time series.

Variables	Time period	Temporal resolution
Precipitation (P) (mm)	1981–2012	Monthly
Streamflow (Q) (m^3/s)	1981–2012	Monthly
Air temperature (T) (°C)	1981–2012	Monthly
Normalized Differential Vegetation Index (NDVI)	1984–2012	Monthly
Evapotranspiration (ET) (mm)	2000–2012	Monthly
Irrigation (IRRI) (Mm^3)	2000–2012	Monthly

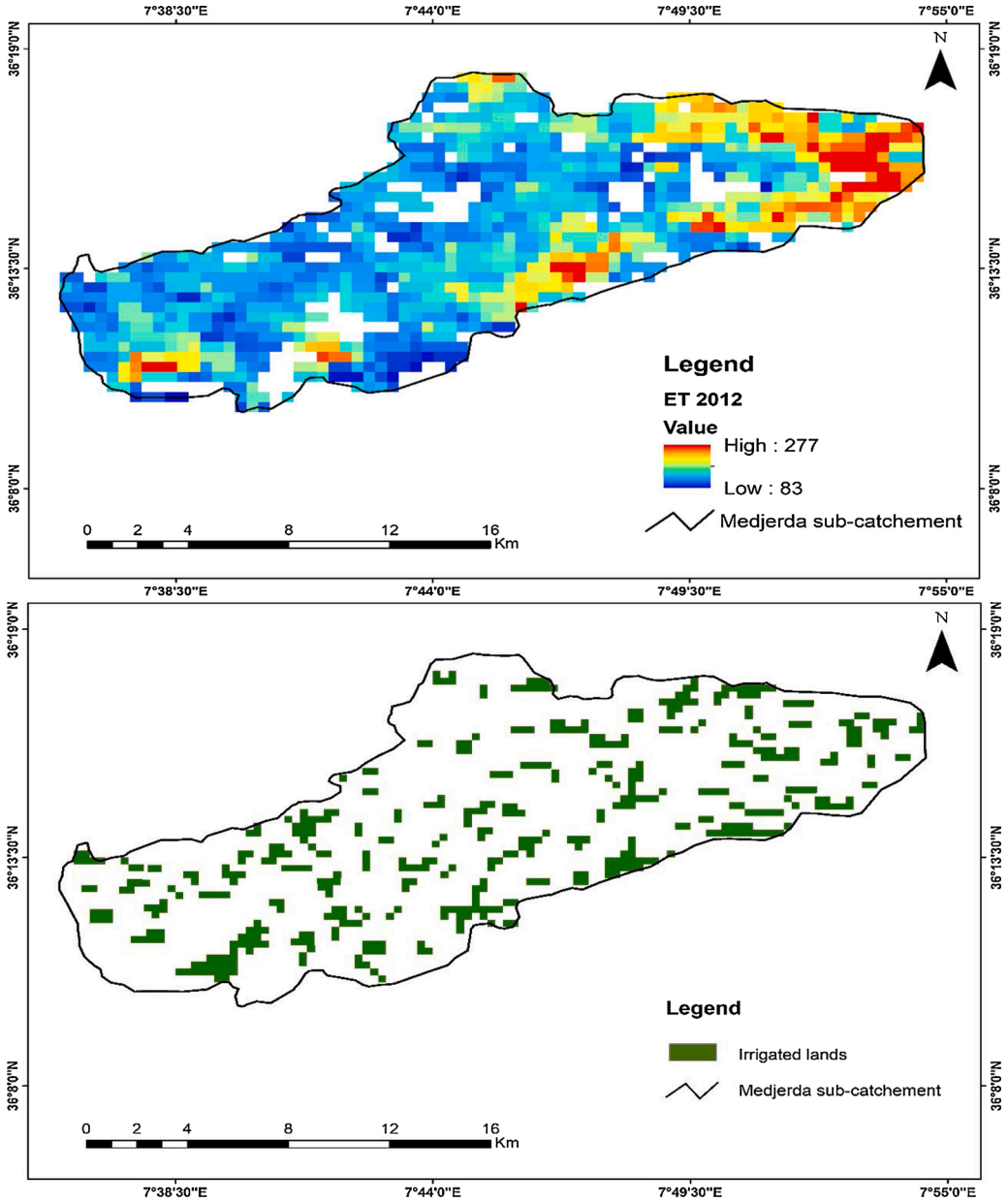

Fig. 2. Mapping and assessing of MODIS-ET (April 2012) (top) and CCI Irrigation Land Cover 2012 (bottom) in the sub-catchment upstream in the Medjerda catchment.

2000−2012. Land cover and evapotranspiration products were resampled at a 100 m spatial resolution in order to reduce processing errors.

Water consumption of irrigated lands in the entire basin was estimated from the product of the average water volume per pixel and the number of pixels (Yang et al., 2018; Fehri et al., 2019) as follows :

$$C_{Irrig,RS=} V_{pp} \times N_p \quad (1)$$

where $C_{Irrig,\ RS}$, indicates water consumption of irrigated land; V_{pp}, average irrigated water per pixel; N_p, the number of pixels.

For the calculation of water consumption, the water efficiency in the Medjerda catchment was considered and added to the estimated volume of evapotranspiration per month from irrigated lands. The irrigation water efficiency in the study area is estimated to range from 55 % to 40 % with a decrease of 1% each year, which signifies that 60 % to 45 % of irrigation water is lost in the system during the period 2000−2012 (MADR, 2018). These losses include field seepage, deep infiltration and conveyance losses in the irrigation system.

3.3. Trend analysis: the Mann–Kendall (MK) test

The nonparametric MK test is applied for the detection of monotonic increasing or decreasing trends in the time series of hydroclimatic variables and possible explaining factors (Su et al., 2018a; Khazaei et al., 2019). The MK test has been widely used for trend analysis of hydrological time series (Mann, 1945; Kendall, 1962; Yue et al., 2002). The slope of the trend is estimated in the time series using the non-parametric method Theil–Sen estimator developed by Sen (1968) and Theil (1992). The MK-test was selected because of its robustness with respect for non-normality. The MK test has further the same power as its parametric competitors (Serrano et al., 1999). The MK statistic S is given by:

$$S = \sum_{i=1}^{n-1} \sum_{j=i+1}^{n} sgn(x_j - x_i); \tag{2}$$

$$sgn(z) = \begin{cases} 1 \; if \; z > 0 \\ 0 \; if \; z = 0 \\ -1 \; if \; z < 0 \end{cases} \tag{3}$$

where x_i and x_j are the data value at times i and j, n is the length of the data set. Under the null hypothesis that x_i are independent and randomly ordered, for n greater than 8, the statistic S is approximately normally distributed with zero mean and variance:

$$Var(S) = \left[n(n-1)(2n+5) - \sum_{i=1}^{n} t_i i(i-1)(2i+5) \right] \Big/ 18 \tag{4}$$

where t_i denotes the number of ties of extent i.

At the significance level (5%), the existing trend is considered to be statistically significant if $p \leq \alpha/2$ in the case of the two-tailed test.

3.4. Convergent Cross Mapping (CCM)

Sugihara et al. (2012) introduced the empirical Convergent Cross Mapping (CCM) causal detection method to identify the causality in complex ecosystems associated with deterministic, low-dimensional and nonlinear dynamics. The CCM method allows identifying causality between a couple of variables in a dynamical system based on nonlinear state-space reconstruction (Takens, 1981). It is based on the reciprocal prediction skills of two variables X and Y. Ye et al. (2015) extended the CCM method to involve time lagged predictions. If X and Y are interconnected in the same dynamical system, the cross-mapping between observed time series variables must converge, which means that the cross-mapping prediction skill improves with increasing library length (Chang et al., 2017). This is due to the fact that more data in the library length produces the reconstructed manifold denser, and the highly resolved attractor gives better accuracy of prediction on neighboring points (Chang et al., 2017). Convergence is therefore considered the main criterion to detect causal interactions (Wang et al., 2018).

Based on a series of simple model experiments, Sugihara et al. (2012) demonstrated that the CCM approach effectively detects mirage correlation and detects underlying causality. A feedback connection can also be considered in CCM approach and allows thus revealing bilateral causality between time series variables (Sliva et al., 2015). The CCM approach is therefore highly suitable for detecting bidirectional relationships between for instance streamflow and meteorological factors.

The CCM is based on Generalized Takens' Theorem saying that it should be possible to cross-predict or cross-map variables that belong to the same dynamical system. Consider two variables, X and Y, that interact in a dynamical system. Then the univariate reconstructions based on X alone should uniquely identify the system state and thus the corresponding value of Y, and vice versa. The CCM method was implemented by using the Empirical Dynamics Modelling package within the R language environment (rEDM: https://cran.rproject.org/web/packages/rEDM/vignettes/rEDM-tutorial.html) (Ye et al., 2015). The analysis was based on monthly time series in the study area. The following parameters are required to run the CCM method: the dimensionality E (i.e. the best embedding dimension needed to reconstruct the attractor), the time delay τ, and the number of nearest neighbor points to use for prediction n. The value of E is varying from 1 or 10. A larger value of E induces more precise convergent maps. The variable nearest neighbors are determined by $E + 1$.

The implementation procedure includes the following steps:

i Standardize data sets

Standardizing a dataset involves rescaling the distribution of values so that the mean of observed values is 0 and the standard deviation is 1. Standardization can be useful and even required in some machine learning algorithms when time series data have input values with different scales.

ii Identify embedding dimension

The best embedding dimension of the attractor is determined by evaluating the attractor's prediction skill for different embedding

dimensions. The prediction is done by using simplex projection using a nonlinear forecasting algorithm developed by Sugihara and May (1990).

The identification of the optimal embedding dimension (E) is computed using simplex projection technique from the rEDM package to individual time series. In this method, the ability of one variable to predict its own dynamics is estimated using different embedding dimensions values of E, ranging from 1 to 10. The correlation coefficient ρ between predictions and observations represents the forecast skill, and the optimal embedding dimension corresponds to the highest forecast skill selected by plotting predictability with respect to the embedding dimension. In our case, CCM analysis was computed using $E = 6$, and $\tau = 1$.

iii Run Convergent Cross Mapping using the CCM function.

Let's consider two time series variables X and Y, and let's consider that they interact in the same dynamical system affected by a deterministic nonlinear process. If a variable X is found to causally drive variable Y, then the signature about X should be encoded into the variable Y. The CCM method looks on to the time-lagged affected variable Y to see if it allows predicting the time-lagged causal variable X. Using the delayed Y coordinates (My) as lagged values of the affected variable, the Y attractor of the original manifold which governs the dynamics of Y is reconstructed. From the reconstructed shadow manifold of Y, if it is possible to predict the time series of X, then the CCM algorithm concludes that Y is indeed driven by X. To test the predictability, the nearest neighbor method, called simplex projection, is used. In order to differentiate between correlation and causation, a measurement of convergence is therefore used.

The following parameters are considered: L: the time series length; the time series variable X: $\{X\} = \{X(1), X(2), \ldots X(L)\}$; the time series variable Y: $\{Y\} = \{Y(1), Y(2), \ldots Y(L)\}$; M_x, M_y : the shadow constructed manifolds of X, Y; τ: the time lag; E : the embedding dimension; and $\dot{X}(t)|\ M_y$: the estimated variable X from cross mapping M_y.

The algorithm involves the following steps:

Step 1: Constructing the manifolds M_x, and M_y

The shadow manifolds M_X and M_Y respectively are constructed for both variables X and Y using the embedding dimension E. This means that M_X will be built based on $X(t)$, $X(t\text{-}1)$ and $X(t\text{-}2)$, while M_Y is constructed from $Y(t)$, $Y(t\text{-}1)$ and $Y(t\text{-}2)$.

Step 2: Cross-mapping from M_X to M_Y (X_xmap_Y) or from M_Y to M_X (Y_xmap_X)

This step consists in selecting and locating for each t, y(t) the contemporaneous lagged coordinate vector on M_y and identify its E+1 nearest neighbors points on the attractor. Subsequently the distance matrix measuring Euclidean distances to the reference point is

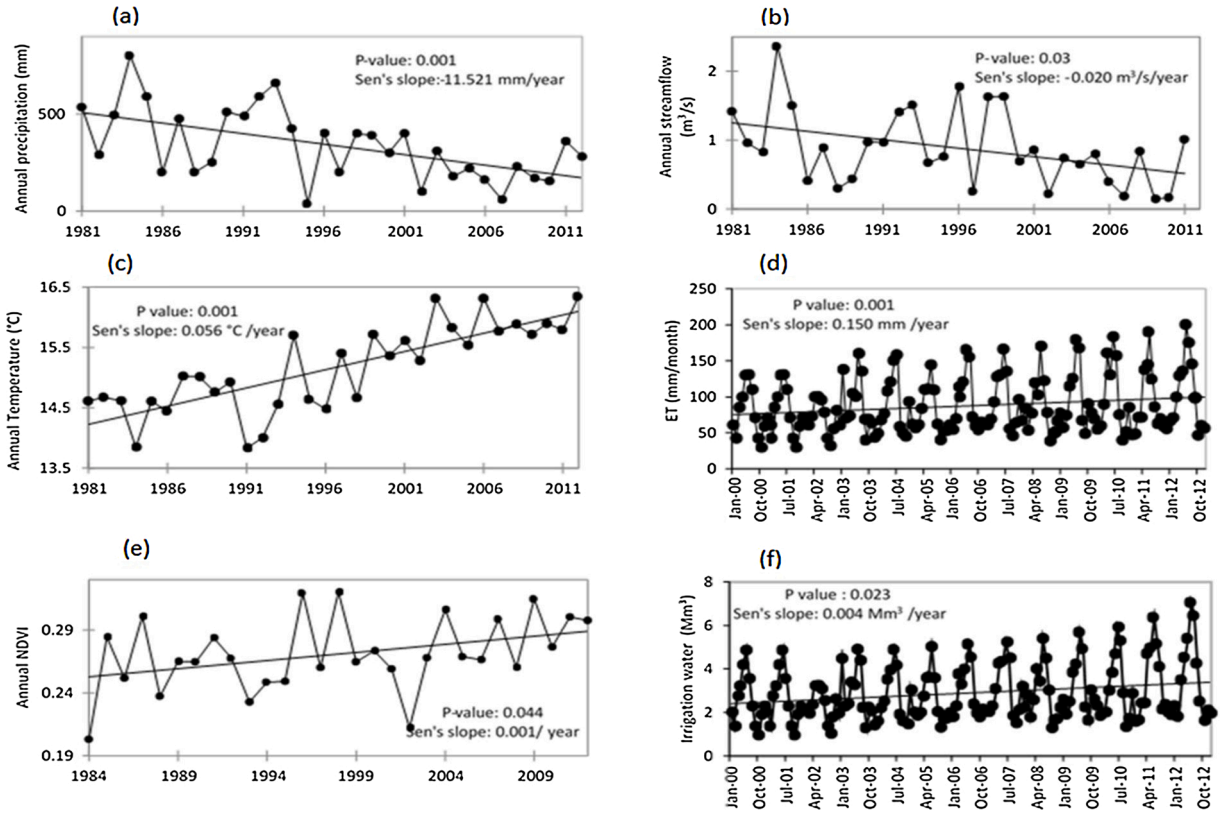

Fig. 3. Results of the MK trend analysis (SL = 0.05) applied to the annual precipitation (a), mean annual streamflow (b), mean annual temperature (c), mean monthly evapotranspiration (d), mean annual NDVI (e), and mean annual water irrigation(f).

calculated. If there is a one to one mapping between M_x and M_y, then the time indices t will detect the nearest neighbor points to M_x and Y is determined to drive X.

Step 3: Affect each of the time indices from the closest to the farthest of y(t) by $t_1,\ldots, t_{E+1}$. These time indices, corresponding to the nearest neighbors to $y(t)$ on M_y, are used to locate points (neighbors) in X *and* to identify $X(t)$ from a locally weighted mean of the $E+1$ $X(t_i)$ values.

Step 4: If the coupled variables interact dynamically, then nearby points in M_x could be able to identify nearby points in M_y. Thus, they are causally related and X is influencing Y. This whole process is conducted with different length size L of the data library.

Step 5: Finally, CCM method is applied to test for causal interaction between variables and assess the extent to which the historical record of the affected variable Y reliably estimates states of a causal variable X, which is measured with the Pearson correlation coefficient between predicted and observed X. If the skill forecast of cross-mapping increases with respect to the library of the time series, the unidirectional causal effect of X on Y can be deduced. The relative level to which predictive skill converges can be interpreted as an estimator of the strength of the causal relationship. Convergence occurs with additional data as the underlying attractor manifold becomes denser, and nearest neighbors get closer.

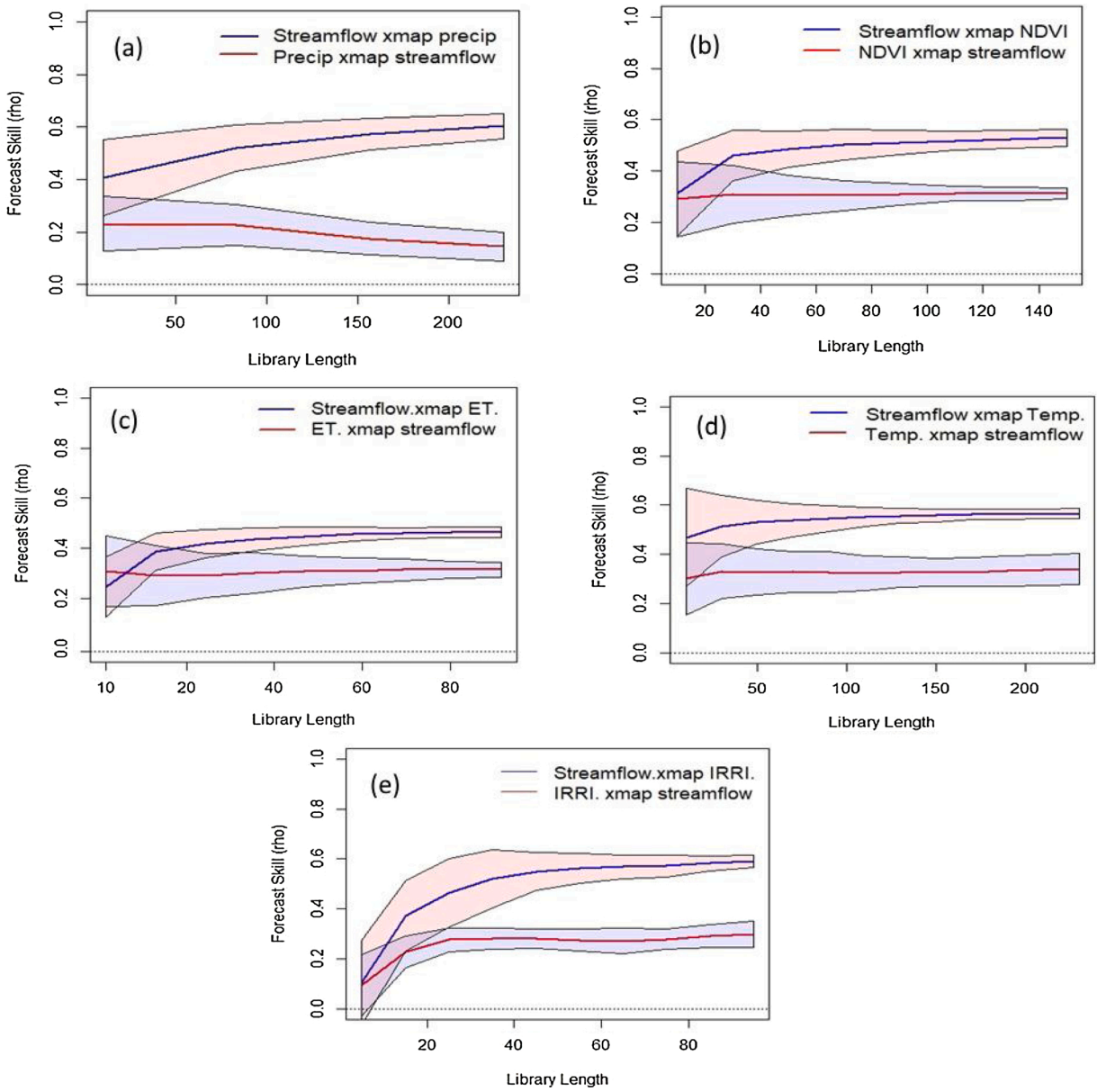

Fig. 4. CCM method results between P, T, ET, NDVI, IRRI, and Q detecting causal relationships on Q. Shaded areas indicate 95 % confidence interval.

In our study, the CCM method has been applied to monthly time series of P, T, ET, NDVI, IRRI, and Q. The causality is consequently revealed if the forecast skill (ρ value) converges with the length L of time series library. Conversely, no causation is detected between the two variables when no convergence appears with increasing library size. The power of influences exerted from one variable on another variable is evaluated by the value of Cross Map skill (ρ value) between estimated and observed values. This skill ranges from 0 to 1. The CCM algorithm was used to explore the causal relationships of P-Q, T-Q, ET-Q, IRR-Q, and NDVI-Q, respectively.

4. Results

4.1. Trend detection analysis

Results of Mann-Kendall trend analysis of streamflow (Q), precipitation (P), temperature (T), evapotranspiration (ET), Normalized Difference of Vegetation Index (NDVI), and irrigation (IRRI) are shown in Fig. 3.

As illustrated in Fig. 3a, a statistically significant downward trend (significance level 5%) is detected for the mean annual of P. The trend magnitude yields -11.5 mm/year across the study area and, therefore, a significant reduction of P has been identified. It reveals that the rainfall pattern is altered over time which is consistent with current climate change projections for the region where precipitation is likely to decrease between 10 and 20 % (Schilling et al., 2012).

Fig. 3b shows that a significant decrease trend is also observed for the annual Q for the period 1981−2012. The trend magnitude assessed by means of the Sen's slope yields -0.020 m^3/s/year. We can therefore confirm that the hydrologic regime of the Medjerda river has been significantly affected during the study period. The consistency between the negative trends of P and Q suggests further that the change in P contributes to the river flow alteration in the upstream region of the Medjerda catchment. Fig. 3c shows a statistically significant upward trend for mean annual temperature from 1981 to 2012. The trend magnitude reaches 0.056 °C / year. This is therefore consistent with the projected rise of temperature between 2 and 3 °C by 2050 as reported by Chourghal et al. (2016). The annual ET trend reported in Fig. 3d, also shows a statistically significant upward trend. The Sens's slope confirms that the ET has increased by about 0.150 mm/year. As shown in Fig. 3e, the mean annual NDVI in the upstream sub-catchment indicates a significant upward trend from 1984 to 2012. The trend magnitude reaches 0.001 / year.

Finally, as shown in Fig. 3f, mean IRRI is also increasing from 2000 to 2012 in the upstream areas of Medjerda. The magnitude of the significant trend in IRRI 0.004 Mm^3/year. The time series of IRRI displays significant seasonal patterns with an increase during spring and summer seasons respectively, followed by decrease in autumn and winter season. The highest value of water consumption in area study was reported in June 2012 (7.057 Mm^3).

4.2. CCM analysis

Forecast skill (ρ value) maps for each possible causal factor of Q are shown in Fig. 4. The estimation forecast skill denoted by ρ value is quantified by calculating the Pearson's correlation coefficient between observed and predicted values.

In dynamical hydrological systems, the causation of P in Q is well known. Fig. 4a confirms that cross-mapping Q from P detects correctly that P drives Q (Fig. 4a). The CCM method exhibits convergence with increasing library length, demonstrating causation between the P and Q ($\rho = 0.59$). Hence, high P in the Medjerda basin is likely to cause high Q. The correlation coefficient for the cross-map of Q from P reach a high value of rho. The significant statistical correlation ($\rho = 0.59$) reveals that P exerts influences on Q directly, as would be expected. In contrast, the cross mapping of P from Q (precipitation xmap streamflow) shows little convergence and therefore the method detects that Q, obviously, does not drive P.

The CCM method detects also that NDVI exerts a moderate influence on Q since the cross-map of Q from NDVI converges to medium value ($\rho = 0.49$). The cross-map NDVI from Q has no significant feedback effect on Q ($\rho = 0.28$) which suggest that the causation of NDVI to Q is unidirectional (Fig. 4b). With respect to ET, Fig. 4c shows that ET also drives Q. Strong convergence is depicted with increasing library length ($\rho = 0.45$). The small feedback also suggests unilateral causation. Unilateral causation implies also that time series of Q in the river holds enough information to predict ET, and hence that the reconstructed manifold of Q contains enough information to predict ET. The CCM method shows further strong convergence with increasing library length between T and Q. Indeed, the correlation coefficient for the cross-map of Q from T reaches a high value of rho ($\rho = 0.56$), while Q has no significant feedback effect on T (Fig. 4d). Convergence suggests therefore that Q is causally forced by T.

With respect to IRRI, Fig. 4e shows that IRRI also drives Q. The CCM algorithm show indeed strong convergence well pronounced with increasing library length between IRRI and Q. Indeed, the CCM also exhibit a strong coupling between the variables within the system (IRRI-Q), as observed by high cross map skills, correlation coefficient for the cross-map of Q from IRRI reach a high value of rho ($\rho = 0.60$), while the cross-map IRRI from Q has a weak feedback effect ($\rho = 0.28$) (Fig. 4e).

Generally, the CCM results show that Q is forced by P, T, ET, NDVI and IRRI and that there are little feedback effects of Q on the possible driving factors.

5. Discussion

5.1. Identification of the hydrological alteration

The results show that the hydrological regime of the upstream part of the Medjerda changed in the past decades. The detected hydrologic alteration will affect and reduce directly the freshwater availability, and increase the trend of extreme events (droughts and

floods) (Ludwig et al., 2011). The streamflow analysis trend using Mann–Kendall test reveals a significant decrease of Q with a magnitude of -0.020 m^3/s/year between 1981 and 2012 (Fig. 3.b). This change is in agreement with the findings of Lespinas et al. (2014) and Sellami et al. (2016) who also revealed significant decreases in annual streamflow over time for their studied Mediterranean catchments. Precipitation time series show also a decreasing trend of -11.521 mm/year (Fig. 3.a) and exhibit a similar dynamic pattern as the streamflow pattern. The alteration of streamflow is indeed generally dominated by precipitation variability (Alkama et al., 2011). According to Dai et al. (2009), precipitation decreased already over many low- and mid-latitude areas, inducing the decrease in streamflow over the period 1948–2004.

The T time series are increasing during the period 1981−2012 with 0.056 °C/year (Fig. 3.c). Increased temperature may support plant growth and may modify the absorption of water and the interception during the growth-phase, which on its turn will influence the infiltration and runoff. As reported by Sellami et al. (2016), results under climate change projections suggest that trends over Mediterranean basins (Southern France and Northeastern Tunisia) are likely to experience a decrease in rainfall regime and increase in air temperature. Our results for the studied catchment upstream of the Medjerda are therefore consistent with these projections.

In coherence with the positive trends of T, ET is also following an increasing trend during the period 2000−2012 (Fig. 3.d). These changes are consistent with the results from Trambaly et al. (2019), who found that Mediterranean basins are under an increase of T and ET over time.

The NDVI time series were used to reflect vegetation change in the sub-catchment of Medjerda. Results obtained from Landsat yield an increasing trend of 0.001/year (Fig. 3.e) during 1984–2012. In contrast to previous factors, positive NDVI trends are mainly attributed to human interventions such as extension farmlands and irrigation activities, which impact the NDVI directly in the studied catchment.

Similarly, irrigation water consumption is following a significant upward trend during the period 2000−2012 with a magnitude of 0.004 Mm^3/year (Fig. 3.f). This is mainly due to the intensive water abstraction dedicated to agriculture, which is the largest economic activity in the region. The irrigation water abstraction is primarily targeted from the Medjerda river as the groundwater resources in the region are overexploited and therefore remain insufficient to support the local agricultural activities.

It is worth noting that, even with robust statistics of the trend analysis of ET and IRRI, these results should be taken with caution since we are dealing with time series of 13 years, which is considered as a relatively short data set for such analysis.

We conclude that the hydrological alteration of Q is concurrent with a decreasing trend in P, and an increasing trend of T, ET, NDVI, and IRRI over time in the study area. However, the relationship may induce complex dynamics. For instance increasing transpiration and evaporation may also increase local P as T and P both interact in the atmosphere system (Gampe et al., 2016). T, and thus these interactions are therefore further investigated with the CCM method to identify and quantify the strength of causal relationships between Q on the one hand, and P, T, ET, NDVI, and IRRI on the other hand.

5.2. *Causal relationships analysis*

The assessment of the causal factors of streamflow using the CCM method show that Q is forced by P, T, ET, NDVI and IRRI. However, it remains difficult to extract one main influential driving force for Q. Despite the fact that the CCM method uses advanced non-linear algorithms to assess the causality and its strengths, it is not easy to discriminate between IRRI, NDVI, ET, P, and T as major driving forcing term on Q alteration. It is also shown that there is feedback of Q on driving factors. Feed-back could be induced by different processes. For instance, when ET increase, local humidity can increase favoring the genesis of local rain. Hence, feed-back mechanisms between driving factors and Q should not be excluded a-priori. Yet, in the studied catchment, the feed-back of Q on possible driving force is rather low, but not negligible. The small feed-back can partially be explained by the size of the study catchment which remains rather small.

As identified in Fig. 4 (a–e), the ρ value increases for P, ET, NDVI, IRR and T with the length of the library. The convergence is pronounced, indicating therefore significant causal effects of P, T, ET, IRRI and NDVI on Q. Hence, based on the CCM prediction procedure measuring the forecast skill of Q on possible driving factors, the causal strengths have been quantified and are significant for all factors. Yet they situate in the same order of magnitude, and currently no robust test value is available to accept or reject the causality based on the strength of the prediction skill.

The significant forecast skill of Q on P reveals, obviously, that P exerts a direct influence on Q, as would be expected. The alteration in the P regime of the studied catchment can therefore produce a significant contribution to the alteration of Q.

The strength of T causing Q is in contrast to the study of Su et al. (2018) who reported that the increase in T has more effect on Q than P. It should also be noted that an increase in T may reduce the relative humidity and hence reduce the probability of rainfall genesis. In the studied catchment, the increased T will not necessarily lead locally to an increased P.

Further, Q is projected to decrease when ET increase (Fig. 3.d) (McCabe and Wolock, 2011). ET is indeed pivotal for studying the hydrological balance, but the impact of ET on Q depends also on the balance between P and ET (Gampe et al., 2016). For instance, the Q alteration in areas where P is largely superior to ET will be less influenced by changes in low P rates. In these cases, Q will be more influenced by changes in high P rates that may induce flooding and increased erosion. This will be different in areas where ET is higher than P, like in our study. In such areas, extreme droughts linked to increasing T could reduce Q. Yet, when P is less than ET, the increase or reduction in P does not necessarily improve (reduce) runoff directly. Similarly, as in our study, Gampe et al. (2016) and Tramblay et al. (2019) explored the impacts of evapotranspiration change on Q in a Mediterranean basins. They found that ET change was the main important driver causing a reduction in soil moisture and annual streamflow.

Further, as described by Moraes et al. (1998), the changes in the land use and land cover, in particular irrigation, can modify the hydrological regime. Indeed, the increase in T in the studied semi-arid region could induce more ET from irrigated croplands,

substantially increasing the demand for water extracted from rivers, dams reservoir, and aquifers for irrigation agriculture. All this, logically, potentially reduces Q. Hence, IRRI played an important role in streamflow reduction, and this has also been confirmed by Zhang et al. (2015), who indicated that the expansion of farmland areas associated with increasing IRRI, leads to declined streamflow. The observed upward trend of IRRI is consistent with population growth in the area during the 2000−2012 period. Such population growth increase the demand for food and water on the national and regional scale (Schilling et al., 2012), and induce a rapid expansion of irrigated lands. Population growth is therefore considered as a driving force in the demand for water, and it has increased rapidly in many areas, especially in Africa, contributing to the decreases in streamflow (Su et al., 2018b). The increased irrigation water abstraction affecting streamflow agree with results found with the study of Gebremicael et al. (2019). They reported that the hydrological alteration of streamflow is attributed to land management change converted into cultivable area in the northern part of Ethiopia, and due to an increase of irrigation water withdrawals.

The joint effect of the different individual factors is more difficult to elucidate with the CCM analysis.

Indeed, the increase of T (Fig. 3.c) and the reduction of P (Fig. 3.a) may jointly cause the observed reduction of Q (Fig. 3.b) in the upstream part of the Medjerda catchment. This would be consistent with the findings of Gampe et al. (2016) who reported that Q is positively correlated with the P and negatively correlated with the T.

Also, the increase of ET's effect in our study cannot be easily separated from T and NDVI's effect. Increasing T may indeed induce a water deficit over irrigated agriculture produced by increasing ET losses, thus increasing plant water stress and desiccation, which influences the vegetation growth through photosynthesis. This would be consistent with the findings of Yuan et al. (2017) who stated that warming trends caused by high T could lead to the increase of potential ET and, finally, a decrease of NDVI, all of which contribute to streamflow alteration.

Yet, it still can be shown that the hydrological alteration of Q can be fairly well explained by direct human activities such as changes in catchment characteristics (including expansion of land cover and land use dynamics). This is consistent with other studies considering that anthropogenic impacts caused by reservoir irrigation, agricultural activity, and channel irrigation exert important influences streamflow alteration considerably (Xue et al., 2017; Zhang et al., 2016, 2015; Miao et al., 2011; Zhang et al., 2010).

6. Conclusion

In this study, the hydrological alteration of streamflow and its causes was explored for the Medjerda upstream sub-catchment (North-East of Algeria) using Mann-Kendall (MK) trend analysis and nonlinear timeseries analysis tool, Convergent Cross Mapping (CCM). The major conclusions are as follows:

(1) The streamflow (Q) in the study area showed a significant decreasing trend during the period 1981–2012 with a magnitude of -0.020 m^3/s/year. Thus, a significant hydrological alteration of the upstream part of the Medjerda river was observed. The trends of possible explanatory factors were also assessed. Similar and different trend behaviors to Q were found, i.e. a decrease of P (-11.521 mm/year), and an increase of T, ET, NDVI, and IRRI with magnitudes of 0.056 °C/year, 0.150 mm/year, 0.001/year, and 0.004 Mm^3/year, respectively.
(2) The causality analysis using CCM revealed causal links between Q and P, T, ET, IRRI and NDVI. The causal link between P and Q were consistent with the decreasing trend of P and Q. The causality between T, ET and Q can be related to the increasing trends of T and ET. Furthermore, a strong causal effect of NDVI and IRRI on Q was observed which also is consistent with the statistical trend analysis.
(3) It is concluded that both climate change and human activities, mainly agricultural development and irrigation, are the dominant causal processes that altered the hydrological regime in the Medjerda river. This suggests the implementation of better operational integrated water resources plans in the region in order to reduce the pressure exerted on the Medjerda river as an important water resource in the North-East Algerian region.

CRediT authorship contribution statement

Mokrane Kadir: Conceptualization, Methodology, Software, Validation, Formal analysis, Data curation, Writing - original draft, Writing - review & editing, Visualization. **Raed Fehri:** Methodology, Writing - original draft, Writing - review & editing. **Doudja Souag:** Supervision, Visualization, Investigation. **Marnik Vanclooster:** Methodology, Writing - review & editing, Supervision.

Declaration of Competing Interest

The authors report no declarations of interest.

Acknowledgments

We acknowledge the support of the Université catholique de Louvain (UCLouvain). This work was supported by the Islamic Development Bank (IDB) under the Excellence Merit Grant [number 36/114367].

Appendix A. Supplementary data

Supplementary material related to this article can be found, in the online version, at doi:https://doi.org/10.1016/j.ejrh.2020.100750.

References

Alkama, R., Decharme, B., Douville, H., Ribes, A., 2011. Trends in global and basin-scale runoff over the late twentieth century: methodological issues and sources of uncertainty. J. Clim. 24, 3000–3014. https://doi.org/10.1175/2010JCLI3921.1.

Barnett, T.P., Adam, J.C., Lettenmaier, D.P., 2005. Potential impacts of a warming climate on water availability in snow-dominated regions. Nature 438, 303–309. https://doi.org/10.1038/nature04141.

Bouraoui, F., Benabdallah, S., Jrad, A., Bidoglio, G., 2005. Application of the SWAT model on the Medjerda river basin (Tunisia). Phys. Chem. Earth 30, 497–507. https://doi.org/10.1016/j.pce.2005.07.004.

Chang, C., Ushio, M., Hsieh, C., 2017. Empirical dynamic modeling for beginners. Ecol. Res. 32, 785–796. https://doi.org/10.1007/s11284-017-1469-9.

Chourghal, N., Lhomme, J.P., Huard, F., Aidaoui, A., 2016. Climate change in Algeria and its impact on durum wheat. Reg. Environ. Change 16, 1623–1634. https://doi.org/10.1007/s10113-015-0889-8.

Cohen Liechti, T., Matos, J.P., Boillat, J.L., Schleiss, A.J., 2014. Influence of hydropower development on flow regime in the Zambezi River Basin for different scenarios of environmental flows. Water Resour. Manag. 29, 731–747. https://doi.org/10.1007/s11269-014-0838-1.

Dai, A., Qian, T., Trenberth, K.E., Milliman, J.D., 2009. Changes in continental freshwater discharge from 1948 to 2004. J. Clim. 22, 2773–2792. https://doi.org/10.1175/2008JCLI2592.1.

Duan, W., Chen, Y., Li, Z., Yang, J., De Maeyer, P., Wang, Y., 2018. Detecting the causal effect of soil moisture on precipitation using convergent cross mapping. Sci. Rep. 8, 1–8. https://doi.org/10.1038/s41598-018-30669-2.

FAO, 2018. SDG Indicator 6.4.2 - Water Stress [WWW Document]. www.fao.org.

Fehri, R., Khlifi, S., Vanclooster, M., 2019. Disaggregating SDG-6 water stress indicator at different spatial and temporal scales in Tunisia. Sci. Total Environ. 694, 133766 https://doi.org/10.1016/j.scitotenv.2019.133766.

Gampe, D., Nikulin, G., Ludwig, R., 2016. Using an ensemble of regional climate models to assess climate change impacts on water scarcity in European river basins. Sci. Total Environ. 573, 1503–1518. https://doi.org/10.1016/j.scitotenv.2016.08.053.

Gao, B., Xu, B., Cai, J., Chen, Z., He, B., Dai, S., Xie, X., 2017. Detecting the causality influence of individual meteorological factors on local PM2.5 concentration in the Jing-Jin-Ji region. Sci. Rep. 7, 1–11. https://doi.org/10.1038/srep40735.

Gebremicael, T.G., Mohamed, Y.A., Van der Zaag, P., 2019. Attributing the hydrological impact of different land use types and their long-term dynamics through combining parsimonious hydrological modelling, alteration analysis and PLSR analysis. Sci. Total Environ. 660, 1155–1167. https://doi.org/10.1016/j.scitotenv.2019.01.085.

Hollmann, R., Merchant, C.J., Saunders, R., Downy, C., Buchwitz, M., Cazenave, A., Chuvieco, E., Defourny, P., de Leeuw, G., Forsberg, R., 2013. The ESA climate change initiative: satellite data records for essential climate variables. Bull. Am. Meteorol. Soc. 94, 1541–1552.

Kendall, M.G., 1962. Rank Correlation Methods. Hafner. Publ. Company, New York.

Khazaei, B., Khatami, S., Alemohammad, H., Rashidi, L., Wu, C., Madani, K., Kalantari, Z., Destouni, G., AghaKouchak, A., 2019. Climatic or regionally induced by humans? Tracing hydro-climatic and land-use changes to better understand the Lake Urmia tragedy. J. Hydrol. 569 https://doi.org/10.1016/j.jhydrol.2018.12.004.

Lespinas, F., Ludwig, W., Heussner, S., 2014. Hydrological and climatic uncertainties associated with modeling the impact of climate change on water resources of small Mediterranean coastal rivers. J. Hydrol. 511, 403–422. https://doi.org/10.1016/j.jhydrol.2014.01.033.

Li, W., Macbean, N., Ciais, P., Defourny, P., Lamarche, C., Bontemps, S., Houghton, R.A., Peng, S., 2018. Gross and net land cover changes in the main plant functional types derived from the annual ESA CCI land cover maps (1992-2015). Earth Syst. Sci. Data Discuss. 10, 219–234. https://doi.org/10.5194/essd-10-219-2018.

Ludwig, R., Roson, R., Zografos, C., Kallis, G., 2011. Towards an inter-disciplinary research agenda on climate change, water and security in Southern Europe and neighboring countries. Environ. Sci. Policy 14, 794–803.

MADR, 2018. Rapport technique de l'irrigation.

Mann, H., 1945. Non-parametric tests against trend. Econometrica 13, 245–259.

McCabe, G.J., Wolock, D.M., 2011. Century-scale variability in global annual runoff examined using a water balance model. Int. J. Climatol. 31, 1739–1748. https://doi.org/10.1002/joc.2198.

Meng, L., Long, D., Quiring, S.M., Shen, Y., 2014. Statistical analysis of the relationship between spring soil moisture and summer precipitation in East China. Int. J. Climatol. 34, 1511–1523. https://doi.org/10.1002/joc.3780.

Miao, C., Yang, L., Liu, B., Gao, Y., Li, S., 2011. Streamflow changes and its influencing factors in the mainstream of the Songhua River basin, Northeast China over the past 50 years. Environ. Earth Sci. 63, 489–499. https://doi.org/10.1007/s12665-010-0717-x.

Milly, P.C.D., Dunne, K.A., Vecchia, A.V., 2005. Global pattern of trends in streamflow and water availability in a changing climate. Nature 438, 347–350. https://doi.org/10.1038/nature04312.

Monteith, J.L., 1965. Evaporation and environment. Symp. Soc. Exp. Biol. 19, 205–234.

Moraes, J.M., Pellegrino, G.Q., Ballester, M.V., Martinelli, L.A., Victoria, R.L., Krusche, A.V., 1998. Trends in hydrological parameters of a southern Brazilian watershed and its relation to human induced changes. Water Resour. Manag. 12, 295–311. https://doi.org/10.1023/A:1008048212420.

Mu, Q., Zhao, M., Running, S.W., 2011. Improvements to a MODIS global terrestrial evapotranspiration algorithm. Remote Sens. Environ. 115, 1781–1800. https://doi.org/10.1016/j.rse.2011.02.019.

Schilling, J., Freier, K.P., Hertig, E., Scheffran, J., 2012. Climate change, vulnerability and adaptation in North Africa with focus on Morocco. Agric. Ecosyst. Environ. 156, 12–26. https://doi.org/10.1016/j.agee.2012.04.021.

Sellami, H., Benabdallah, S., La, I., Vanclooster, M., 2016. Quantifying hydrological responses of small Mediterranean catchments under climate change projections. Sci. Total Environ. 543, 924–936. https://doi.org/10.1016/j.scitotenv.2015.07.006.

Sen, P.K., 1968. Estimates of the Regression Coefficient Based on Kendall's Tau 63, pp. 1379–1389.

Serrano, A., Mateos, V.L., Garcia, J.A., 1999. Trend analysis of monthly precipitation over the Iberian Peninsula for the period 1921–1995. Phys. Chem. Earth, Part B Hydrol. Ocean. Atmos. 24, 85–90.

Sliva, A., Reilly, S.N., Casstevens, R., Chamberlain, J., 2015. Tools for validating causal and predictive claims in social science models. Procedia Manuf. 3, 3925–3932. https://doi.org/10.1016/j.promfg.2015.07.920.

Su, L., Miao, C., Kong, D., Duan, Q., Lei, X., Hou, Q., Li, H., 2018a. Long-term trends in global river flow and the causal relationships between river flow and ocean signals. J. Hydrol. 563, 818–833. https://doi.org/10.1016/j.jhydrol.2018.06.058.

Su, L., Miao, C., Kong, D., Duan, Q., Lei, X., Hou, Q., Li, H., 2018b. Long-term trends in global river flow and the causal relationships between river flow and ocean signals. J. Hydrol. 563, 818–833. https://doi.org/10.1016/j.jhydrol.2018.06.058.

Sugihara, G., May, R.M., 1990. Nonlinear forecasting as a way of distinguishing chaos from measurement error in time series. Nature 344, 734–741. https://doi.org/10.1038/344734a0.

Sugihara, G., May, R., Ye, H., Hsieh, C., Deyle, E., Fogarty, M., Munch, S., 2012. Detecting Causality in Complex Ecosystems. https://doi.org/10.1126/science.1227079.

Takens, F., 1981. Detecting strange attractor in turbulance. Dyn. Syst. Turbul. 366–381. https://doi.org/10.1007/bfb0091924.

Theil, H., 1992. A rank-invariant method of linear and polynomial regression analysis. Henri Theil's Contributions to Economics and Econometrics. Springer, pp. 345–381.

Tramblay, Y., Mimeau, L., Neppel, L., Vinet, F., Sauquet, E., 2019. Detection and attribution of flood trends in Mediterranean basins. Hydrol. Earth Syst. Sci. Discuss. 23, 4419–4431. https://doi.org/10.5194/hess-23-4419-2019.

Van Nes, E.H., Scheffer, M., Brovkin, V., Lenton, T.M., Ye, H., Deyle, E., Sugihara, G., 2015. Causal feedbacks in climate change. Nat. Clim. Change 5, 445–448. https://doi.org/10.1038/nclimate2568.

Wang, G., Zhang, N., Fan, K., Palus, M., 2018. Central European air temperature: driving force analysis and causal influence of NAO. Theor. Appl. Climatol. https://doi.org/10.1007/s00704-018-2676-1.

Xue, L., Zhang, H., Yang, C., Zhang, L., Sun, C., 2017. Quantitative assessment of hydrological alteration caused by irrigation projects in the Tarim River basin. China. Sci. Rep. 7, 1–13. https://doi.org/10.1038/s41598-017-04583-y.

Yang, P., Xia, J., Zhan, C., Mo, X., Chen, X., Hu, S., Chen, J., 2018. Estimation of water consumption for ecosystems based on vegetation interfaces processes model: a case study of the Aksu river basin, Northwest China. Sci. Total Environ. 613–614, 186–195. https://doi.org/10.1016/J.SCITOTENV.2017.09.045.

Ye, H., Deyle, E.R., Gilarranz, L.J., Sugihara, G., 2015. Distinguishing time-delayed causal interactions using convergent cross mapping. Sci. Rep. 5, 1–9. https://doi.org/10.1038/srep14750.

Yuan, X., Wang, W., Cui, J., Meng, F., Kurban, A., De Maeyer, P., 2017. Vegetation changes and land surface feedbacks drive shifts in local temperatures over Central Asia. Sci. Rep. 7, 3–10. https://doi.org/10.1038/s41598-017-03432-2.

Yue, Sheng, Pilon, Paul, Cavadias, George, 2002. Power of the Mann±Kendall and Spearman's rho tests for detecting monotonic trends in hydrological series. J. Hydrol. 259, 254–271.

Zamoum, S., Souag-Gamane, D., 2019. Monthly streamflow estimation in ungauged catchments of northern Algeria using regionalization of conceptual model parameters. Arab. J. Geosci. 12 https://doi.org/10.1007/s12517-019-4487-9.

Zhang, Q., Xu, C.Y., Tao, H., Jiang, T., Chen, Y.D., 2010. Climate changes and their impacts on water resources in the arid regions: A case study of the Tarim River basin, China. Stoch. Environ. Res. Risk Assess. 24, 349–358. https://doi.org/10.1007/s00477-009-0324-0.

Zhang, A., Zheng, C., Wang, S., Yao, Y., 2015. Analysis of streamflow variations in the Heihe River Basin, northwest China: trends, abrupt changes, driving factors and ecological influences. J. Hydrol. Reg. Stud. 3, 106–124. https://doi.org/10.1016/j.ejrh.2014.10.005.

Zhang, H., Huang, Q., Zhang, Q., Gu, L., Chen, K., Yu, Q., 2016. Changes in the long-term hydrological regimes and the impacts of human activities in the main Wei River, China. Hydrol. Sci. J. 61, 1054–1068. https://doi.org/10.1080/02626667.2015.1027708.

Zhao, W., Chang, Xuexiang, Chang, Xueli, Zhang, D., Liu, B., Du, J., Lin, P., 2018. Estimating water consumption based on meta-analysis and MODIS data for an oasis region in northwestern China. Agric. Water Manag. 208, 478–489. https://doi.org/10.1016/j.agwat.2018.06.035.